

Interfacial magnetism in manganite superlattices

Kalpataru Pradhan, Arno P. Kampf

Angaben zur Veröffentlichung / Publication details:

Pradhan, Kalpataru, and Arno P. Kampf. 2013. "Interfacial magnetism in manganite superlattices." *Physical Review B* 88 (11): 115136.
<https://doi.org/10.1103/physrevb.88.115136>.

Nutzungsbedingungen / Terms of use:

licgercopyright

Dieses Dokument wird unter folgenden Bedingungen zur Verfügung gestellt: / This document is made available under the following conditions:

Deutsches Urheberrecht

Weitere Informationen finden Sie unter: / For more information see:

<https://www.uni-augsburg.de/de/organisation/bibliothek/publizieren-zitieren-archivieren/publizieren>



Interfacial magnetism in manganite superlattices

Kalpataru Pradhan and Arno P. Kampf

Center for Electronic Correlations and Magnetism, Theoretical Physics III, Institute of Physics, University of Augsburg,
D-86135 Augsburg, Germany

(Received 14 June 2013; revised manuscript received 13 September 2013; published 23 September 2013)

We use a two-orbital double-exchange model including superexchange interactions, Jahn-Teller lattice distortions, and long-range Coulomb interactions to investigate the origin of magnetically disordered interfaces between ferromagnetic metallic (FM) and antiferromagnetic insulating (AFI) manganites in FM/AFI superlattices. The induced magnetic moment in the AFI layer varies nonmonotonically with increasing AFI layer width as seen in the experiment. We provide a framework for understanding this nonmonotonic behavior which has a one-to-one correspondence with the magnetization of the FM interface. The obtained insights provide a basis for improving the tunneling magnetoresistance in FM/AFI manganite superlattices by avoiding a magnetic dead layer in the FM manganite.

DOI: [10.1103/PhysRevB.88.115136](https://doi.org/10.1103/PhysRevB.88.115136)

PACS number(s): 75.47.Lx, 75.70.Cn, 85.30.Mn, 85.75.Dd

The ferromagnetic metallic (FM) manganites have emerged as potential candidates for spintronics devices^{1,2} due to their high spin polarization.^{3,4} For the future generation of magnetic tunnel junctions (MTJs) artificial trilayers of insulating metal oxides sandwiched between FM manganites are currently designed. In MTJs a large tunneling magnetoresistance (TMR)⁵ is observed by switching the spin orientation in the FM leads from antiparallel to parallel configurations; the TMR is defined by the ratio $(R_{AP} - R_P)/R_P$ where R_{AP} and R_P are the resistances for antiparallel and parallel orientations, respectively.⁶ Although SrTiO₃ is predominantly used as the insulator between La_{0.67}Sr_{0.33}MnO₃ (LSMO) layers, other combinations of FM and non-magnetic insulating (NMI) oxides [FM = LSMO, La_{0.67}Ca_{0.33}MnO₃ (LCMO); NMI = TiO₂, LaAlO₃, NdGaO₃] have also been tested for their performance.⁷⁻¹⁰

TMR is a spin-dependent process which critically depends on the magnetic and the electronic properties of the interface between FM manganites and the insulating material.¹ In such a spin-sensitive device it is required to have a structurally and magnetically well defined interface. It is an experimental fact that the magnetization of FM manganites decreases at the interface below its bulk value,¹¹ the origin of which is not well understood. The reduction of the magnetization at the interface, usually referred to as the magnetic dead layer (MDL),^{8,9} has an adverse effect on the TMR by decreasing the tunneling current, which by itself should be large for device applications. A recent microscopic analysis¹² suggests that the decrease of the double-exchange energy at an FM/SrTiO₃ interface is the origin of the MDL. The possible coexistence of different magnetic phases at the interface is however not accessible from such an analysis.

The reduction of the magnetization has been attributed to phase separation, and/or electronic and magnetic reconstructions due to structural inhomogeneities at the interface. Unlike at the surface of FM manganites³ it is a difficult task to determine the electronic and structural changes at interfaces which are several nanometers below the surface. To minimize disorder and strain effects isostructural interfaces are favorable. In a different approach NMI barriers were replaced by antiferromagnetic insulating (AFI) manganites.¹³⁻¹⁶ In the presence of

a small external magnetic field not only the FM manganites align but there is a likely possibility that the magnetization in the AFI layer also aligns along the FM leads.^{13,15} Specifically the relation between the magnetoresistance and the induced magnetic moment in the AFI barrier was established in LSMO/Pr_{0.67}Ca_{0.33}MnO₃(PCMO)/LSMO superlattices.¹⁷ The magnetic moment of the PCMO layers in the superlattice behaves nonmonotonically with increasing PCMO layer width.¹³ Remarkably the magnetoresistance follows a very similar nonmonotonic behavior. It is *a priori* not clear from the LSMO/PCMO/LSMO superlattices whether MDLs at the interface exist for different widths of the PCMO layers.

In this paper, we explore in detail the electronic and magnetic reconstructions of the FM/AFI superlattices at the electron density $n = 0.5$ for different widths of the AFI layers. Electrons are transferred from the FM to the AFI layers at the interface even though the initial electron density in the bulk materials are equal. The amount of electron transfer from the FM interfacial line depends upon the thickness of the AFI layer. We explain the nonmonotonic behavior of the induced ferromagnetic moment in the AFI layer with increasing AFI layer width and establish explicitly a one-to-one correspondence between the induced magnetic moment in the AFI layer and the magnetization at the interface in the FM/AFI superlattices. This concept establishes a route to minimize or even avoid the MDL in FM/AFI superlattices.

We consider a two-dimensional model Hamiltonian for manganite superlattices composed of alternating FM and AFI regions. The model and the method we employ have been elaborately discussed in Ref. 18. The model is given by

$$H = H_{\text{FM}} + H_{\text{AFI}} + H_{\text{LRC}}, \quad (1)$$

where both H_{FM} and H_{AFI} have the same reference Hamiltonian¹⁹⁻²²

$$H_{\text{ref}} = \sum_{(ij)\sigma} \sum_{\alpha\beta} t_{\alpha\beta}^{ij} c_{i\alpha\sigma}^\dagger c_{j\beta\sigma} - J_H \sum_i \mathbf{S}_i \cdot \boldsymbol{\sigma}_i + J \sum_{(ij)} \mathbf{S}_i \cdot \mathbf{S}_j - \lambda \sum_i \mathbf{Q}_i \cdot \boldsymbol{\tau}_i + \frac{K}{2} \sum_i \mathbf{Q}_i^2 - \mu \sum_{i\alpha\sigma} c_{i\alpha\sigma}^\dagger c_{i\alpha\sigma}. \quad (2)$$

H_{ref} is constructed to reproduce the correct sequence of magnetic phases in the bulk limit.^{22,23} J_H is the Hund's rule coupling between t_{2g} spins \mathbf{S}_i and the e_g electron spin σ_i , and J is the antiferromagnetic (AF) superexchange between the t_{2g} spins. λ measures the strength of the coupling between the e_g electron and the Jahn-Teller phonons in the adiabatic limit.

We treat all t_{2g} spins and lattice degrees of freedom as classical²⁴ and measure energies in units of the Mn-Mn hopping $t_{aa} = t$. In manganites t is approximately 0.2–0.5 eV.²⁵ The estimated value of J_H is 2 eV,²⁶ i.e., much larger than t . For this reason we further adopt the limit $J_H \rightarrow \infty$.²⁰ We also set $K = 1$ and $|\mathbf{S}_i| = 1$. In an external magnetic field a Zeeman coupling $H_{\text{mag}} = -\mathbf{h} \cdot \sum_i \mathbf{S}_i$ is added to the Hamiltonian.

The average electron density of the constituent FM and AFI manganites in the FM/AFI superlattices is fixed by choosing the same chemical potential μ . The long-range Coulomb (LRC) interaction between all the charges, essential to control the amount of charge transferred across the interface, is taken into account via a self-consistent solution of the Coulomb potentials ϕ_i at the mean-field level by setting^{27–29} $\phi_i = \alpha t \sum_{j \neq i} \frac{\langle n_j \rangle - Z_j}{|\mathbf{R}_i - \mathbf{R}_j|}$ in the long-range Coulomb part of the Hamiltonian, $H_{\text{LRC}} = \sum_i \phi_i n_i$. It is assumed that all the point charges Z_j from the background ions are fixed and confined to the Mn sites. $\langle n_j \rangle$ refers to the e_g electron density at the Mn site \mathbf{R}_j . The Coulomb interaction strength is controlled by the parameter $\alpha = e^2/\epsilon a t$ where ϵ and a denote the dielectric constant and the lattice parameter, respectively. For the 2D case considered here α is approximately 0.1.¹⁸

We apply an exact diagonalization scheme to the itinerant electron system for each configuration of the background classical variables of the t_{2g} spins and the lattice distortions. We use a Monte Carlo sampling technique based on the “traveling cluster approximation” (TCA).³⁰ TCA for superlattices has been discussed in Ref. 18.

Here we analyze specifically superlattices composed of FM and AFI manganites of equal electron density $n = 0.5$. We use the typical value $J = 0.1$ ^{22,31} for both the FM and the AFI manganites and differentiate between a FM and an AFI phase by varying λ . For the parameters $J = 0.1$ and $n = 0.5$, the ground state is a FM for $\lambda \equiv \lambda_M = 1.0$ while it is an AFI for $\lambda \equiv \lambda_I \geq 1.6$. The AFI phase at $n = 0.5$ is a charge- and orbital-ordered *CE* phase.²² The density of states is finite for the FM phase while it is gapped at the Fermi level for the AFI phase; charge transfer from the FM to the AFI side is expected when the FM and the AFI are joined together.

An FM/AFI superlattice is shown schematically in Fig. 1. The width of the AFI spacer, sandwiched between the FM layers, is denoted by w . Periodic boundary conditions are enforced in both directions to represent a superlattice structure composed of alternating FM and AFI regions. The type I superlattice is considered in the following discussions while results for the type II superlattice are briefly discussed in the concluding paragraphs.

Different combinations of electron-phonon couplings ($\lambda_M = 1.0$, $\lambda_I = 1.6$ –2.0) are considered first in the absence of LRC interactions $\alpha = 0$. To start with we discuss the results for $\lambda_I = 1.65$ [see Fig. 2(a)], for which the ferromagnetic structure factor $\langle S_I(\mathbf{0}) \rangle$ behaves nonmonotonically with increasing

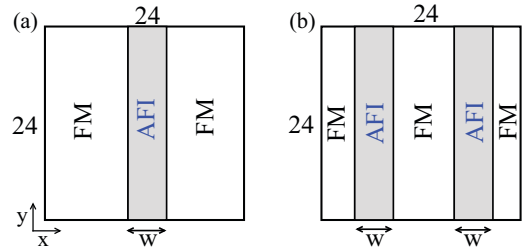


FIG. 1. (Color online) Schematic view of the FM/AFI superlattice on a 24×24 lattice. (a) Type I: One AFI layer. (b) Type II: Two AFI layers. We consider periodic boundary conditions in both directions.

AFI layer width, where $S_I(\mathbf{q}) = \frac{1}{N_I} \sum_{i,j \in \text{AFI}} \mathbf{S}_i \cdot \mathbf{S}_j e^{i\mathbf{q} \cdot (\mathbf{r}_i - \mathbf{r}_j)}$ and the angular bracket denotes the thermal average combined with an additional average over ten different “samples.” The induced magnetization in the AFI layer is small for $w = 1$, nearly equal to 1 (all the t_{2g} spins are fully ordered) for $w = 2$, and rapidly decreases for $w > 7$.

The averaged z component of the t_{2g} spins $\langle S_{zI} \rangle$ in the AFI layer for $\lambda_I = 1.65$ is nonmonotonic similarly to $\langle S_I(\mathbf{0}) \rangle$ as shown in Fig. 2(b). We also measure the local staggered charge order by $\langle CO_I \rangle = \frac{1}{N_I} \sum_{i \in \text{AFI}} \langle n_i \rangle e^{i(\pi, \pi) \cdot \mathbf{r}_i}$ where i denotes one of the N_I lattice sites in the AFI layer with position \mathbf{r}_i . $\langle CO_I \rangle$, shown in Fig. 2(b), remains small for $w \leq 7$ and starts to rise for $w > 7$. The decrease in the magnetization accompanied by the emerging charge order indicates that the AFI layer gradually returns to the bulk AFI state with increasing w .

$\langle S_I(\mathbf{0}) \rangle$ for different λ_I values also varies nonmonotonically with increasing width of the AFI layer except for $\lambda_I = 2.0$. The induced magnetic moment for $w > 2$ decreases more rapidly for larger electron-phonon coupling λ_I . The AFI layer recovers

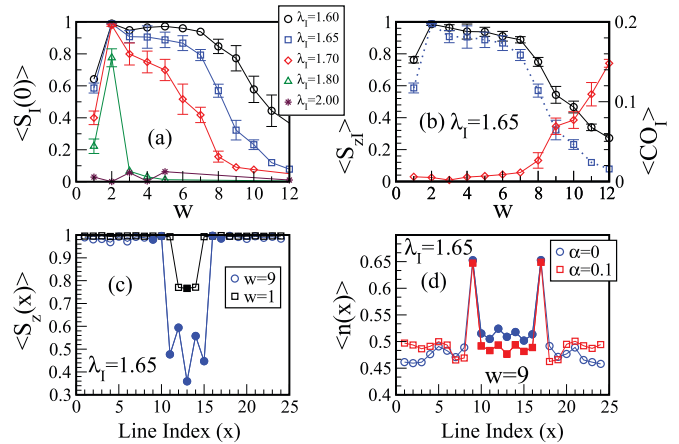


FIG. 2. (Color online) (a) Ferromagnetic structure factor $\langle S_I(\mathbf{0}) \rangle$ for different widths of the AFI layer at $T = 0.01$ ($\lambda_M = 1.0$ and $\lambda_I = 1.6$ –2.0). (b) Average z component of the t_{2g} spins, $\langle S_{zI} \rangle$, and the average staggered charge order $\langle CO_I \rangle$ (see text) in the AFI layer for $\lambda_M = 1.0$ and $\lambda_I = 1.65$. $\langle S_I(\mathbf{0}) \rangle$ is also included as the dotted line. (c) Line-averaged z component of the t_{2g} spins $\langle S_z(x) \rangle$ for $w = 9$ and $w = 1$. (d) Line-averaged electron density $\langle n(x) \rangle$ for $w = 9$ with ($\alpha = 0.1$) and without ($\alpha = 0.0$) LRC interactions. In (c) and (d) open and closed symbols are from lines in the FM and the AFI layers, respectively.

the AF, charge-ordered state at a smaller width w for larger λ_I . It is therefore easier to induce a ferromagnetic moment in large-bandwidth (small λ) manganites. This is why it is possible to magnetize only 2 lines of the AFI layer for $\lambda_I = 1.8$ while for $\lambda_I = 2.0$ the induced magnetic moment remains very small in the AFI layer irrespective of its width.

In order to understand the nonmonotonic behavior we specifically choose $w = 1$ and $w = 9$ for which $\langle S_I(\mathbf{0}) \rangle$ is small. To start with we analyze the magnetization profile across the interface by calculating average magnetization for each line of the superlattice $\langle S_z(x) \rangle$ for transverse coordinate x . $\langle S_z(x) \rangle$, in Fig. 2(c), decreases for $x = 11-15$ for $w = 9$, i.e., in the center lines of the AFI layer, which implies that the induced ferromagnetic moment in the AFI layer is confined to the near vicinity of the interface. The relation between the induced magnetization and the line-averaged electron density $\langle n(x) \rangle$ becomes evident in Fig. 2(d). $\langle n(x) \rangle$ for the interfacial line on the FM side, named as FM interfacial line, decreases while the AFI interfacial line increases from the initial electron density 0.5 to ~ 0.65 . The induced ferromagnetic moment for the lines $x = 9$ and 17 is therefore due to the enhanced electron density and the spin bias from the ferromagnetic metal. In fact, for the parameters $J = 0.1$, $n = 0.65$, and $\lambda_I = 1.65$ the ground state of the bulk system is a FM. The magnetization in the line $x = 10$ (16) is induced by the fully magnetized line $x = 9$ (17). The interfacial lines of the AFI layer are also magnetized for other w values, except for $w = 1$, which is discussed later. The spin bias from the ferromagnetic metal is important for the induction of a ferromagnetic moment in the AFI interfacial lines. The induced magnetization in the AFI layer is very small irrespective of the AFI layer width where the FM interfacial lines are magnetically disordered.¹⁸

The direction of electron transfer is from the FM to the AFI layer as anticipated earlier. Sufficiently far away from the interface the average electron density must return to the initial electron density $n = 0.5$, which however is not fully accomplished for $w = 9$ and $\alpha = 0$. But with the additional LRC interaction $\langle n(x) \rangle$ indeed gradually returns to the initial electron density [see Fig. 2(d)]. For $\alpha = 0.1$ the electron densities are clearly lower (higher) in the AFI (FM) layer as compared to $\alpha = 0$. In the FM/AFI superlattices, where the constituent FM and AFI manganites have the same initial electron density, the LRC interaction reduces the critical width, beyond which $\langle S_I(\mathbf{0}) \rangle$ starts to decrease.¹⁸ Remarkably, $\langle n(x) \rangle$ at the FM interfacial lines is largely unaltered by the LRC interactions.

The line-averaged $\langle S_z(x) \rangle$ for $w = 1$ is also shown in Fig. 2(c). But in contrast to the AFI layer width $w = 9$, $\langle S_z(x) \rangle$ in the FM interfacial line decreases for $w = 1$. The difference results from the decrease in the electron density for $w = 1$ in the FM interfacial line as shown in Fig. 3(a). The spin pattern in the interfacial line decomposes into FM and G-type AF regions. This is shown in Fig. 3(b) which displays the averaged z components of the t_{2g} spins $\langle S_z(y) \rangle$ for each site of the FM interfacial line $x = 12$ for one selected “sample.”

The averaged electron density at the FM interfacial line is smaller for $\lambda_I = 1.70$ as compared to $\lambda_I = 1.65$ as shown in Fig. 3(a). For this reason the G-type AF regions in the FM interfacial line are more pronounced for $\lambda_I = 1.70$ [see Fig. 3(d)]. The electron densities and the z components of the

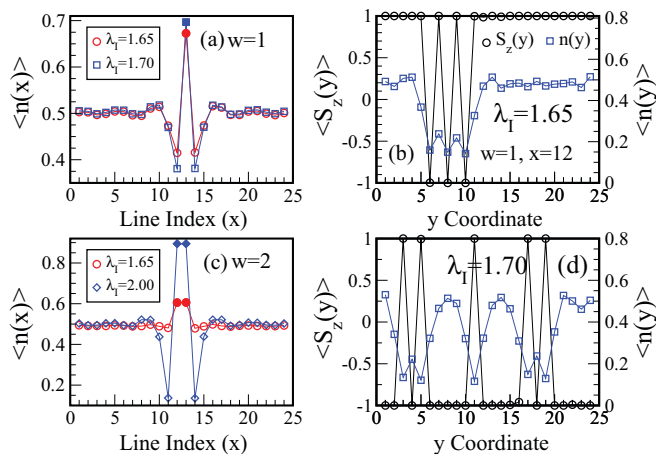


FIG. 3. (Color online) Line-averaged electron density $\langle n(x) \rangle$ for (a) $w = 1$, (c) $w = 2$. The z component of the t_{2g} spins $\langle S_z(y) \rangle$ and $\langle n(y) \rangle$ for each site of the FM interfacial line $x = 12$ for $w = 1$ using (b) $\lambda_I = 1.65$ and (d) $\lambda_I = 1.70$. Legends in (b) and (d) are the same. Open and closed symbols in (a) and (c) are from the FM and the AFI layers, respectively.

t_{2g} spins at each site in the superlattice are shown in Fig. 4 for $w = 1$. The magnetic and the electronic profile of both FM interfacial lines are similar to each other on both sides of the AFI line. The magnetic profile of the AFI line is tied to the profile of the FM interfacial lines while the electron density of the sites in the AFI layer is enhanced to ~ 0.7 .

With increasingly larger values of λ_I the magnetization of the FM interfacial line decreases due to the enhanced G-type correlations for $w = 1$. This establishes the crucial relation between the magnetization at the FM interfacial line and the induced magnetic moment in the AFI layer. This is in general true for any width w . So the nonmonotonic behavior of $\langle S_I(\mathbf{0}) \rangle$ in Fig. 2(a) implies that the FM interfacial line remains ferromagnetic for $w = 2$. For $w = 2$ the decrease in the electron density in the FM interfacial line [see Fig. 3(c), $\lambda_I = 1.65$] is very small as compared to $w = 1$, and these lines therefore remain ferromagnetic. For $\lambda_I = 1.80$ the electron density in the FM interfacial line decreases considerably except for $w = 2$. The electron density profile for $w = 2$ and $\lambda_I = 1.80$ resembles the profile of $w = 2$ and $\lambda_I = 1.65$ shown in Fig. 3(c). This implies that the charge transfer

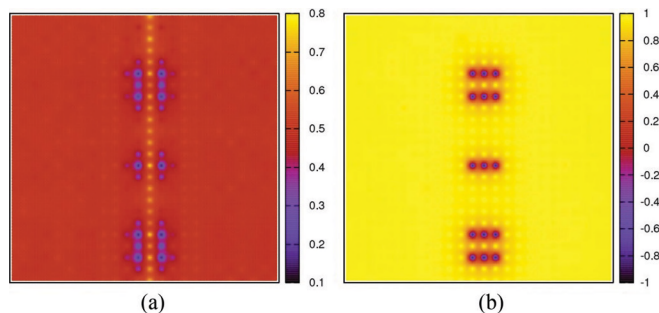


FIG. 4. (Color online) (a) The electron densities and (b) the z components of the t_{2g} spins for each site on a 24×24 superlattice at $T = 0.01$ with the AFI layer width $w = 1$ ($\lambda_M = 1.0$ and $\lambda_I = 1.7$).

across the interface from the FM to the AFI layer also varies nonmonotonically similarly to the induced magnetic moment in the AFI layer shown in Fig. 2(a). The competition between FM and G-type AF spin patterns at the interface is controlled by the double-exchange energy gain due to the induced magnetic moment in the AFI layer. The magnetization of the FM interfacial layer remains ferromagnetic for $w = 2$; i.e., the large induced magnetic moment in the AFI layer removes the MDL.

At large electron-phonon couplings $\lambda_I \gtrsim 2.0$ electrons are site localized due to strong lattice distortions; this decreases the double-exchange energy gain from induced ferromagnetic moments which are hence absent in the AFI layer [see Fig. 2(a)] irrespective of the AFI layer width. For this reason G-type spin patterns are more prominent at the FM interfacial lines and $\langle n(x) \rangle$ in the FM interfacial line decreases considerably [see, e.g., Fig. 3(c) for $w = 2$ and $\lambda_I = 2.0$]. These results suggest that also in FM/NMI superlattices local AF correlations may emerge in the FM interfacial line and the magnetization at the interface is wiped out originating in an MDL due to the decrease in the electron density at the interface.^{8,9}

In the type I FM/AFI superlattices the spins in the FM leads are aligned in the same direction due to the periodic boundary conditions; this setup mimics the experimental situation in which the FM layers of the superlattice are aligned by an external magnetic field. Specifically we have designed the type II superlattice where two AFI layers instead of one are considered as shown in Fig. 1(b) to represent more closely the experimental setup. The magnetizations in the left and the right FM layers are aligned parallel while the middle FM layer is free to choose its spin direction. A small external magnetic field h is applied to align all the FM layers in the same direction. Figure 5(a) shows the line averaged $\langle n(x) \rangle$ vs line index x for $w = 1$, $\lambda_I = 1.8$, and $h = 0.002$. In Fig. 5(b), we plot the averaged $\langle S_{zI} \rangle$ in the AFI layers along with averaged z component of the t_{2g} spins in the FM interfacial lines $\langle S_z(IL) \rangle$ for the same magnetic field. The magnetization of the FM interfacial line follows a nonmonotonic behavior similar to the induced magnetic moments in the AFI layer. The dc limit of the longitudinal conductivity σ_{dc} , also displayed in Fig. 5(b), as obtained from the Kubo-Greenwood formula,^{32,33} follows the same trend with increasing AFI layer width w . It is the combination of the induced magnetic moment in the AFI layer and the magnetization of the FM interfacial lines which enhances the conductivity.

In the type II setup the TMR may be calculated by fixing the spins of the middle FM layer in the direction opposite to that of the left and right FM layers. However in the limit $J_H \rightarrow \infty$ adopted here where the spins of the mobile e_g electrons are perfectly aligned along the local t_{2g} spin

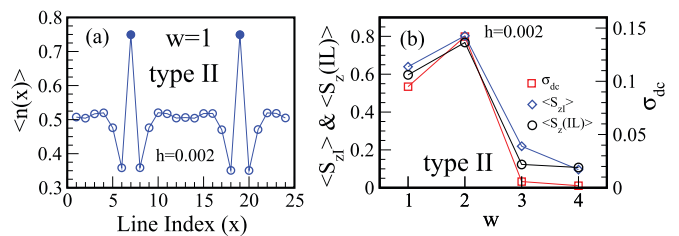


FIG. 5. (Color online) Type II FM/AFI superlattice ($\lambda_M = 1.0$ and $\lambda_I = 1.8$): (a) Line-averaged electron density $\langle n(x) \rangle$ for $w = 1$. (b) $\langle S_{zI} \rangle$, $\langle S_z(IL) \rangle$ (see text), and the dc conductivity (in units of $\pi e^2/h a$ where a is the lattice spacing; see Ref. 33) at $T = 0.01$ for different AFI layer widths w . An external magnetic field $h = 0.002$ is applied to align the FM layers.

direction the dc conductivity (resistivity) for this setup is zero (infinity). For this reason a quantitative calculation of TMR for different widths w of the AFI layer is not presented here. In the experiments the resistivity is large but finite in the antiparallel configuration of the FM layers. The increase of the conductivity in the parallel configuration of the FM layers, shown in Fig. 5(b), will necessarily enhance the TMR.

In conclusion, our 2D model calculations provide a framework to explain the origin of the MDL at the FM interface in FM/insulator superlattices. The magnetization of the interfacial lines of the FM layers is determined by the amount of electron transfer from the FM interfacial lines to the AFI layer. The decrease in the magnetization of the FM interface, when joined with a NMI oxide, is due to the decrease in the electron density at the interfacial lines as a result of the charge transfer across the interface. The amount of transferred charge is limited in a scenario for which instead AFI layers are sandwiched between FM layers, since inducing a ferromagnetic moment in the AFI layer requires controlling the charge transfer. But even in such a FM/AFI superlattices, the MDL is absent only for a specific range of AFI layer widths, because the induced magnetic moment in the AFI layer varies nonmonotonically with the AFI layer width.¹³ The absence of the MDL in FM/AFI superlattices enhances the TMR. The MDL at the interface in an FM/NMI junction may be minimized by the insertion of an intervening AFI layer. In such a setup, the width of the AFI layer has to be chosen such that the AFI layer is maximally polarized along the direction of the magnetization in the FM layers due to charge transfer. Indeed the TMR is significantly enhanced in the engineered FM/NMI MTJs with an intervening AFI layer.^{34,35} The role of the MDL for different widths of the intervening AFI layer in these engineered MTJs deserves further investigation. We leave this as the subject for future work.

This work was supported by the Deutsche Forschungsgemeinschaft through TRR 80.

¹J. M. De Teresa, A. Barthélemy, A. Fert, J. P. Contour, F. Montaigne, and P. Seneor, *Science* **286**, 507 (1999).

²M. Bibes and A. Barthélemy, *IEEE Trans. Electron Devices* **54**, 1003 (2007).

³J.-H. Park, E. Vescovo, H.-J. Kim, C. Kwon, R. Ramesh, and T. Venkatesan, *Nature (London)* **392**, 794 (1998).

⁴*Colossal Magnetoresistive Oxides*, edited by Y. Tokura (Gordon and Breach, New York, 2000).

- ⁵M. Bowen, M. Bibes, A. Barthélémy, J. P. Contour, A. Anane, Y. Lemaître, and A. Fert, *Appl. Phys. Lett.* **82**, 233 (2003).
- ⁶M. Julliere, *Phys. Lett. A* **54**, 225 (1975).
- ⁷J. Z. Sun, W. J. Gallagher, P. R. Duncombe, L. Krusin-Elbaum, R. A. Altman, A. Gupta, Yu Lu, G. Q. Gong, and Gang Xiao, *Appl. Phys. Lett.* **69**, 3266 (1996).
- ⁸J. Z. Sun, D. W. Abraham, R. A. Rao, and C. B. Eom, *Appl. Phys. Lett.* **74**, 3017 (1999).
- ⁹M. Bibes, L. Balcells, S. Valencia, J. Fontcuberta, M. Wojcik, E. Jedryka, and S. Nadolski, *Phys. Rev. Lett.* **87**, 067210 (2001).
- ¹⁰V. Garcia, M. Bibes, A. Barthélémy, M. Bowen, E. Jacquet, J. P. Contour, and A. Fert, *Phys. Rev. B* **69**, 052403 (2004).
- ¹¹J. W. Freeland, J. J. Kavich, K. E. Gray, L. Ozuyzer, H. Zheng, J. F. Mitchell, M. P. Warusawithana, P. Ryan, X. Zhai, R. H. Kodama, and J. N. Eckstein, *J. Phys.: Condens. Matter* **19**, 315210 (2007).
- ¹²M. B. Lepetit, B. Mercey, and C. Simon, *Phys. Rev. Lett.* **108**, 087202 (2012).
- ¹³D. Niebieskikwiat, L. E. Hueso, J. A. Borchers, N. D. Mathur, and M. B. Salamon, *Phys. Rev. Lett.* **99**, 247207 (2007).
- ¹⁴R. Cheng, K. Li, S. Wang, Z. Chen, C. Xiong, X. Xu, and Y. Zhang, *Appl. Phys. Lett.* **72**, 2475 (1998).
- ¹⁵H. Li, J. R. Sun, and H. K. Wong, *Appl. Phys. Lett.* **80**, 628 (2002).
- ¹⁶M. Jo, M. G. Blamire, D. Ozkaya, and A. K. Petford-Long, *J. Phys.: Condens. Matter* **15**, 5243 (2003).
- ¹⁷D. Niebieskikwiat, L. E. Hueso, N. D. Mathur, and M. B. Salamon, *Appl. Phys. Lett.* **93**, 123120 (2008).
- ¹⁸K. Pradhan and A. P. Kampf, *Phys. Rev. B* **87**, 155152 (2013).
- ¹⁹S. Yunoki, T. Hotta, and E. Dagotto, *Phys. Rev. Lett.* **84**, 3714 (2000).
- ²⁰E. Dagotto, T. Hotta, and A. Moreo, *Phys. Rep.* **344**, 1 (2001).
- ²¹S. Kumar, A. P. Kampf, and P. Majumdar, *Phys. Rev. Lett.* **97**, 176403 (2006).
- ²²K. Pradhan, A. Mukherjee, and P. Majumdar, *Phys. Rev. Lett.* **99**, 147206 (2007).
- ²³K. Pradhan, A. Mukherjee, and P. Majumdar, *Europhys. Lett.* **84**, 37007 (2008).
- ²⁴E. Dagotto, S. Yunoki, A. L. Malvezzi, A. Moreo, J. Hu, S. Capponi, D. Poilblanc, and N. Furukawa, *Phys. Rev. B* **58**, 6414 (1998).
- ²⁵Z. Popovic and S. Satpathy, *Phys. Rev. Lett.* **88**, 197201 (2002).
- ²⁶Y. Okimoto, T. Katsufuji, T. Ishikawa, A. Urushibara, T. Arima, and Y. Tokura, *Phys. Rev. Lett.* **75**, 109 (1995).
- ²⁷S. Okamoto and A. J. Millis, *Phys. Rev. B* **70**, 075101 (2004).
- ²⁸S. Yunoki, A. Moreo, E. Dagotto, S. Okamoto, S. S. Kancharla, and A. Fujimori, *Phys. Rev. B* **76**, 064532 (2007).
- ²⁹J. Salafranca, M. J. Calderon, and L. Brey, *Phys. Rev. B* **77**, 014441 (2008).
- ³⁰S. Kumar and P. Majumdar, *Eur. Phys. J. B* **50**, 571 (2006).
- ³¹T. G. Perring, G. Aeppli, Y. Moritomo, and Y. Tokura, *Phys. Rev. Lett.* **78**, 3197 (1997).
- ³²G. D. Mahan, *Quantum Many Particle Physics* (Plenum Press, New York, 1990).
- ³³S. Kumar and P. Majumdar, *Eur. Phys. J. B* **46**, 237 (2005).
- ³⁴H. Yamada, Y. Ogawa, Y. Ishii, H. Sato, M. Kawasaki, H. Akoh, and Y. Tokura, *Science* **305**, 646 (2004).
- ³⁵Y. Ishii, H. Yamada, H. Sato, H. Akoh, Y. Ogawa, M. Kawasaki, and Y. Tokura, *Appl. Phys. Lett.* **89**, 042509 (2006).